Hydroxyl Radical Generation Through the Fenton-Like Reaction of Hematin- and Catechol-Functionalized Microgels

Pegah Kord Forooshani[1], Rattapol Pinnaratip[1], Elizabeth Polega[1], Ariana G. Tyo[1], Eric Pearson[2], Bo Liu[1], Tinu-Ololade Folayan[2], Lei Pan[2], Rupak M. Rajachar[1], Caryn L. Heldt[2], Bruce P. Lee[1*]

[1]Department of Biomedical Engineering, Michigan Technological University, Houghton, MI 49931, USA

[2]Department of Chemical Engineering, Michigan Technological University, Houghton, MI 49931, USA

ABSTRACT: Hydroxyl radical (•OH) is a potent reactive oxygen species with the ability to degrade hazardous organic compounds, kill bacteria, and inactivate viruses. However, an off-the-shelf, portable, and easily activated biomaterial for generating •OH does not exist. Here, microgels were functionalized with catechol, an adhesive moiety found in mussel adhesive proteins, and hematin (HEM), a hydroxylated Fe^{3+} ion-containing porphyrin derivative. When the microgel was hydrated in an aqueous solution with physiological pH, molecular oxygen in the solution oxidized catechol to generate H_2O_2, which was further converted to •OH by HEM. The generated •OH was able to degrade organic dyes, including orange II and malachite green. Additionally, the generated •OH was antimicrobial against both gram-negative (*Escherichia coli*) and gram-positive (*Staphylococcus epidermidis*) bacteria with the initial concentration of 10^6-10^7 CFU/mL. These microgels also reduced the infectivity of a non-enveloped porcine parvovirus and an enveloped bovine viral diarrhea virus by 3.5 and 4.5 log reduction values, respectively (99.97-99.997% reduction in infectivity). These microgels were also functionalized with positively charged [2-(methacryloyloxy)ethyl] trimethylammonium chloride (METAC), which significantly enhanced the antibacterial and antiviral activities through electrostatic interaction between the negatively charged pathogens and the microgel. These microgels can potentially serve as a lightweight and portable source of disinfectant, for an on-demand generation of •OH with a wide range of applications.

1. Introduction

Reactive oxygen species (ROS), such as hydrogen peroxide (H_2O_2), superoxide ($O_2^{\cdot-}$), and hydroxyl radical (•OH), are highly reactive chemical species resulting from the reduction of molecular oxygen (O_2).[1] H_2O_2 can decompose in the presence of Fe^{2+} ions to form the highly reactive •OH in a process known as the Fenton reaction.[2, 3] •OH is a nonselective and potent oxidant that immediately reacts with a broad range of organic and hazardous compounds leading to their degradation and elimination from the environment.[4] It is also capable of attacking almost all types of biomolecules in cells including lipids, proteins and amino acids, which can ultimately kill bacteria and inactivate viruses.[5, 6] Additionally, stimulating the •OH generation in bacteria has been reported as the primary mechanism used by antibacterial drugs, such as norfloxacin, ampicillin, and kanamycin.[7]

Fenton and Fenton-like reactions are simple reactions with environmentally friendly byproducts for producing •OH for different applications, including soil remediation and wastewater treatment.[8, 9] However, off-the-shelf formulations for on-demand production of •OH are difficult to achieve due to the slow rate of metal ion oxidation (Fe^{3+} to Fe^{2+}) and extremely short half-life of the generated •OH (10^{-9} s) in solutions.[10, 11] Different approaches have been employed to improve the applicability of the Fenton reaction, including the use of UV light (photo-Fenton), electricity (electro-Fenton), and a reducing agent such as hydroxylamine to accelerate metal ion oxidation.[11-13] However, these systems are expensive, require strict pH control (acidic condition), require bulky equipment (e.g., UV light, electrochemical cells), and require storing a large volume of diluted H_2O_2.

Catechol, an adhesive moiety found in mussel adhesive proteins, autoxidizes to form semiquinone and quinone by one- and two-electron oxidation, respectively (Scheme 1A).[14, 15] During the oxidation process, a considerable amount of ROS, such as $O_2^{\cdot-}$ and H_2O_2, are generated as byproducts.[16-18] Previously, we prepared catechol-functionalized microgel, which converted molecular O_2 in solution to H_2O_2, which demonstrated antimicrobial and antiviral properties.[19] However, H_2O_2 is not a potent disinfectant and the generated H_2O_2 was only effective against an initial bacteria concentration of 10^5 colony forming unit (CFU)/mL. Bacteria such as *Staphylococcus* secretes antioxidant enzymes such as catalase that decomposes H_2O_2,[20] which reduces the antimicrobial efficacy of H_2O_2.

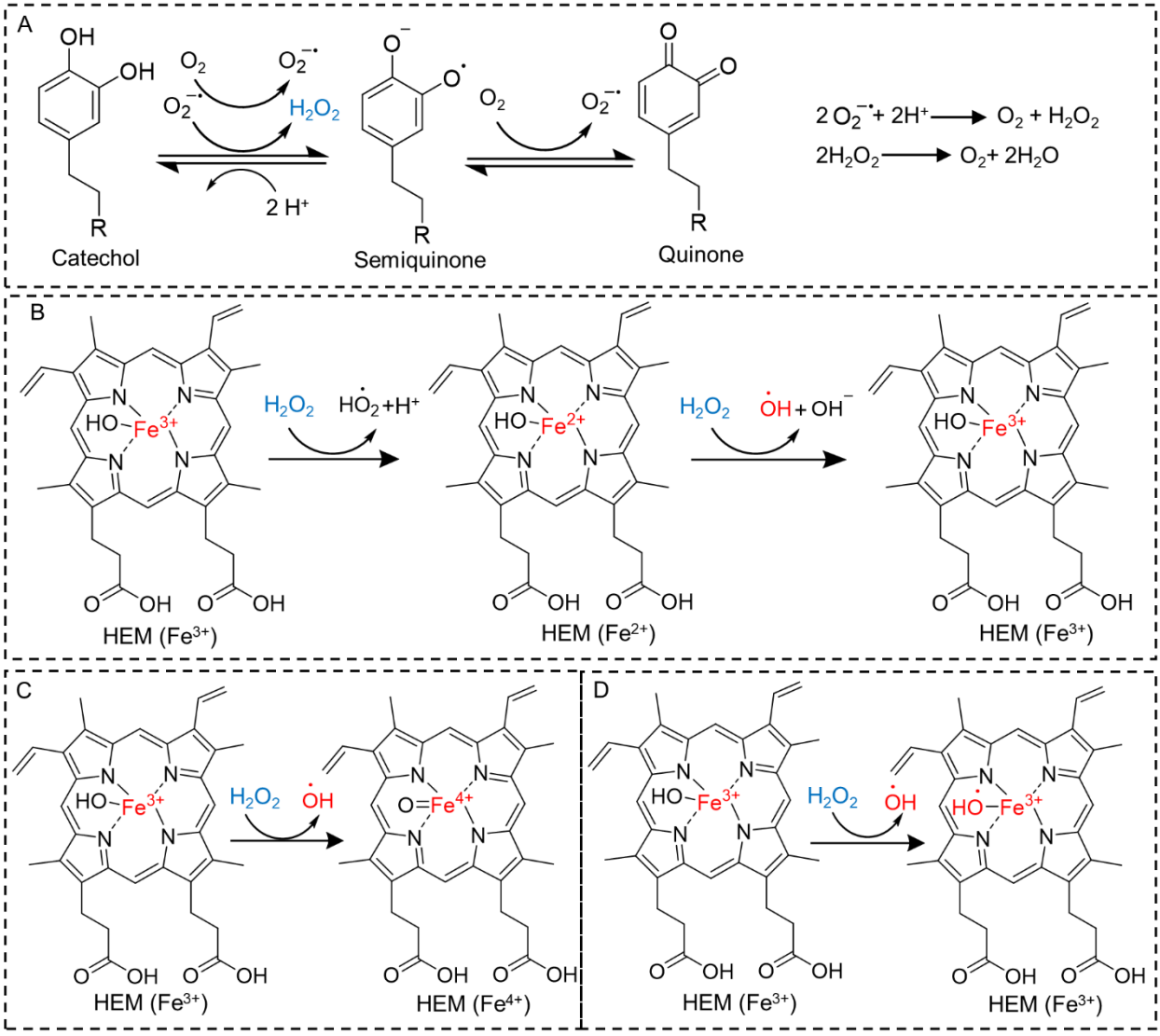

Scheme 1. Proposed mechanism of catechol oxidation and H_2O_2 generation (A), and possible mechanisms of H_2O_2 decomposition and ·OH generation in the presence HEM (B-D).

Here, we seek to engineer an easily-activated and portable biomaterial that can generate highly reactive ·OH by simple hydration in an aqueous solution. To this end, we combined H_2O_2-generating catechol moiety with hematin (HEM) to create microgels for robust antipathogenic and bioremediation applications. HEM is a porphyrin derivative that contains a hydroxylated Fe^{3+} ion.[21] HEM is an inexpensive biomolecule that has been previously demonstrated to catalyze the conversion of H_2O_2 to ·OH.[9, 22, 23] Although the mechanism of conversion is still controversial, some of the possible mechanisms are shown in Scheme 1B-D. However, H_2O_2 needed to be separately added to generate ·OH, which is impractical.

To eliminate the need for separately adding H_2O_2, we immobilized HEM on the surface of dopamine methacrylamide (DMA)-functionalized microgels (Figure 1). DMA contains a catechol moiety that converts O_2 into H_2O_2 through autoxidation when the microgel is hydrated in an aqueous solution. HEM can further convert the generated H_2O_2 to ·OH. The microgels were further functionalized with a cationic monomer, [2-(methacryloyloxy)ethyl] trimethylammonium chloride (METAC), to improve antipathogenic activities through electrostatic interaction between the positively charged microgels and the negatively charged pathogens.[24, 25] The ability of the microgels to generate H_2O_2 and ·OH, degrade organic dyes, kill both gram-positive (*Staphylococcus epidermidis, S. epi*) and gram-negative (*Escherichia coli, E. coli*) bacteria, and inactivate both non-enveloped porcine parvovirus (PPV) and enveloped bovine viral diarrhea virus (BVDV) were investigated.

2. Material and method

2.1. Materials

N-(3-aminopropyl)methacrylamide hydrochloride (APMA), METAC, N-hydroxyethyl acrylamide (HEAA), TWEEN®80, SpanTM80, orange II sodium salt (OII), acetone, porcine hematin (HEM), triethylamine, phosphate buffer saline (PBS,

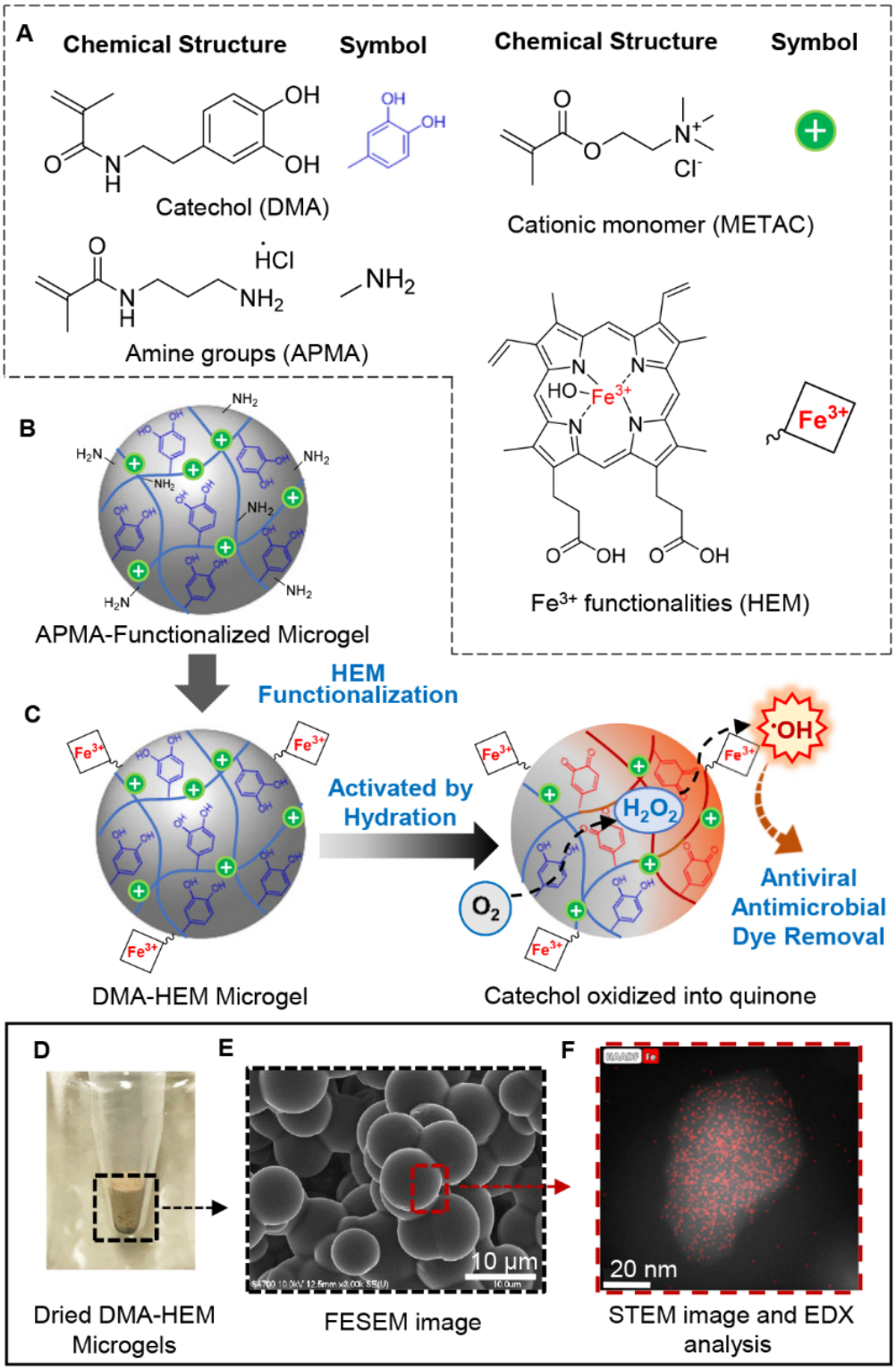

Figure 1. Chemical structure of monomers used to prepare DMA- and HEM-containing microgels (A). APMA-functionalized microgels was first prepared with primary amine groups, which can be further modified with HEM through carbodiimide chemistry (B). Schematic representation of the activation of DMA- and HEM-incorporated microgel to generate •OH for antipathogenic activities and dye degradation (C). When the microgels are hydrated in a neutral pH solution, catechol autoxidation generates H_2O_2, which was subsequently converted to •OH by HEM. Photograph (D) and FESEM (E) images of microgels. SEM-EDX confirmed HEM functionalization based on the presence of iron (red dots) on the surface of the microgels (F).

BioPerformance certified, pH 7.4), and Whatman® qualitative filter paper (Grade 1) were purchased from Sigma Aldrich (St Louis, MO). 1-Hydroxybenzotriazole (HOBt), and O-(benzotriazol-1-yl)-N,N,N′,N′-tetramethyluronium hexafluorophosphate (HBTU) were purchased from Chem-Impex International Inc. (Wood Dale, IL). Methylene bis-acrylamide (MBAA), sodium phosphate dibasic anhydrous, sodium phosphate monobasic monohydrate, and malachite green chloride (MG, technical grade) were obtained from Acros Organics (Fair Lawn, New Jersey). VA-086 was purchased from Wako Chemicals (Richmond, VA). Dimethyl sulfoxide (DMSO), isopropyl alcohol (IPA), and hexanes were purchased from VWR (Radnor, PA). 12 M hydrochloric acid (HCl) and *N*,*N*'-dimethylformamide (DMF) were purchased from Fisher Scientific (Pittsburg, PA). Chloroform was purchased from J.T.Baker (Phillipsburg, NJ). Pierce Quantitative Peroxide Assay Kit with sorbitol, and hydroxyphenyl fluorescein (HPF) was obtained from Thermo Scientific (Rockford, IL). Tryptic soy broth (TSB), Mueller Hinton Agars (28 mL fill, 15×100 mm), and astral inoculation loop (10 µL, sterilized) were obtained from Hardy Diagnostics (Santa Maria, CA). 3-(4,5-dimethyl-2-thiazolyl)-2,5-diphenyl-2H-tetrazolium bromide (MTT) was purchased from Alfa Aesar (Haverhill, MA). BVDV was obtained from USDA APHIS, and PPV was a generous gift of Dr. Ruben Carbonell, from North Carolina State University. Bovine turbinate cells (BT-1, CRL-1390), porcine kidney cells (PK-13, CRL-6489), *E. coli* (ATCC 11775), and *S. epi* (ATCC 12228) were obtained from American Type Culture Collection (ATCC, Manassas, Virginia). Anprolene gas sterilization and gas refills (ethylene oxide) were obtained from Andersen Sterilizers, Inc. (Haw River, NC). DMA was synthesized following the previously published protocols.[26] 0.1 M sodium phosphate buffer (PB, pH 7.4) was prepared by mixing 0.2 M stock solutions of sodium phosphate dibasic and sodium phosphate monobasic, which diluted down to a 0.1 M PB using DI water.[27] Fe^{3+} solution was prepared by diluting 5 mM stock solution of $FeCl_3$ in acidic DI water (pH 3, adjusted by sulfuric acid) to 50 µM using PB (final pH 7.4).[28] HEM solutions were prepared by diluting a 10 mM stock solution of HEM in DMSO to 10 µM solutions using PB (final pH 7.4).

2.2. Preparation of microgels

Microgels were prepared in two steps (Figure S1). During the first step, DMA-containing microgels were prepared with APMA, an $–NH_2$ containing monomer, following published protocol with some modifications.[19] In the second step, APMA-functionalized microgels were further functionalized with HEM through carbodiimide chemistry.

To prepare APMA-functionalized microgel, precursor solutions were prepared by mixing 1 M of HEAA with DMA (0 and 10 mol%), 10 mol% APMA, METAC (0 and 10 mol%), 6 mol % MBAA and 4 mol % VA086 relative to 1 M HEAA in DI water. The polymer precursor solutions were transferred to a rubber plug-sealed flask with a stopcock, frozen for 30 min and degassed three times by backfilling with nitrogen. Surfactant mixture was prepared by adding 500 µL SpanTM80 and 100 µL TWEEN®80 to 70 mL hexanes, in a rubber plug-sealed flask and stirred vigorously under a nitrogen stream for 30 min. Then, the precursor solutions were transferred to the surfactant mixture drop by drop using a syringe. The mixture was stirred vigorously for another 10 min under a nitrogen stream. The reaction mixture was irradiated using UV light (365 nm, UVP UVGL-25, Analytik Jena) from the side of the flask for 4 h and 30 min. Microgels were collected using filter paper and washed with acetone and IPA to obtain white microgels. The microgels were dried under vacuum for overnight and further washed with acidic DI water (pH 3.5) three times. Finally, the microgels were lyophilized to obtain white dried powder. These APMA-functionalized microgels were denoted as HEAA-METAC and DMA-METAC based on the composition of the polymer precursor solution. For example, DMA-METAC contains 10 mol% DMA and 10 mol% METAC. Control microgels that contain 0 and 10 mol% DMA are denoted as HEAA-m and DMA-m, respectively.

APMA-functionalized microgels were further modified with HEM using carbodiimide chemistry. 20 mg HEM (HEM: APMA-incorporated into the microgels = 1:0.1 mol) was dissolved in 7.2 mL DMF and sonicated for 25 min. HBTU, HOBt (HEM:HBTU:HOBt = 1:2:1 mol), and 12.8 mL of chloroform were added to the HEM solution and stirred for 10 min. 400 mg of the APMA-functionalized microgels were added to the reaction mixture, rubber plug-sealed, and stirred under a nitrogen stream for another 10 min. Triethylamine (triethylamine: HEM = 1:1 mol) was added to the reaction mixture using a syringe and further stirred for 1, 4, or 24 h at 25 °C. Finally, microgels were collected by centrifugation at 5000 rpm for 15 min and washed with DMF, DMSO, and acidic water (pH 3.5) in succession until the solution became clear. The collected microgels were lyophilized for 24 h to yield a dried powder. The microgels were denoted as DMA-HEM-1h, DMA-HEM-4h, or DMA-HEM-24h based on the HEM-functionalization reaction time. For example, DMA-HEM-24h indicates the microgels contain 10 mol% DMA, which was further reacted with HEM for 24 h. Similarly, microgels functionalized with DMA, METAC, and HEM are denoted as DMA-METAC-HEM-1h, DMA-METAC-HEM-4h, or DMA-METAC-HEM-24h in the same manner.

2.3. Characterization of microgels

The HEM-functionalized microgels were characterized using ATR-Fourier transform infrared (ATR-FTIR) spectroscopy (Shimadzu IRTracer-100) with a scan rate of 800 scans per minute at the resolution of 1 cm^{-1}. Chemical mapping analysis of dried microgels was performed using the FEI 200kV Titan Themis scanning transmission electron microscopy (STEM) in conjunction with energy dispersive x-ray spectroscopy (EDX). The specimens were prepared by crushing dried microgels in an agate mortar followed by depositing the dry particles on standard copper TEM grids. Thermogravimetric analysis (TGA) was performed on an SDT Q600 instrument with a heating rate of 10 °C/min under nitrogen atmosphere. To estimate the content of Fe in the microgel, TGA was performed on HEM to find the remaining mass at 700°C, which was 64.3 wt% (**Table S1**). Based on the chemical structure of HEM, Fe accounts for only 8.8 wt% of HEM or 13.7 wt% of the remaining mass in the microgels.

The particle size of microgels was determined in both dried and swollen states. Dried microgels were coated with 2 nm thick Pt/Pd coating and characterized using a field emission scanning electron microscope (FESEM, Hitachi S-4700). Dried microgels were hydrated in PBS (pH 7.4) at a concentration of 10

mg/mL and incubated for 24 h at 25 °C. Then, 10 μL of the microgel suspension was dropped onto a glass slide and covered with a coverslip. The microgels were imaged under a light microscope (EVOS M7000, Waltham, MA). The size of the swollen microgels was measured using ImageJ. The values of five pictures were averaged to obtain reliable measurements, and the values are reported as mean ± standard deviation (SD). The swelling ratio was calculated according to the equation below:[29]

$$swelling\ ratio = \frac{V_w - \bar{V}_d}{\bar{V}_d}$$

where V_w is the volume of the swollen microgels and $\bar{V}_d$ is the average volume of the dried microgels calculated assuming the microgel as spheres. Zeta potential analysis of microgels was performed using a Malvern Zetasizer Nano series. 25 mg of microgels were suspended in 3 mL of DI water and sonicated for 5 min before the analysis. The experiment was conducted in a triplet, and the results are reported as mean ± SD.

2.4. H_2O_2 concentration determination

25 mg of microgels were hydrated in 750 μL of PBS (pH 7.4) and incubated for up to 48 h at 37 ˚C with gentle agitation on a shaking plate. Quantitative Peroxide Assay Kit (i.e., ferrous oxidation−xylenol orange (FOX) assay) was used to quantify the H_2O_2 concentration, following the published protocol.[30] A series of solutions containing 0–1 mM of H_2O_2 was used to prepare a standard curve. The experiment was conducted in a triplet, and the results are reported as mean ± SD.

Safety Hazard: H_2O_2 is a strong to moderate oxidizer depending on the concentration. It can be corrosive and cause burn if come to contact with skin and eyes. It can be corrosive to the respiratory system.

2.5. •OH determination using HPF

25 mg of microgels were hydrated in 750 μL of PB (pH 7.4), and 3 μL of HPF (20 μM) was added to the microgel suspension while protected from ambient light. The microgel suspension was incubated for up to 72 h at 37 °C (in the dark) with gentle agitation on a shaking plate. Microgels were separated by centrifugation at 8000 rpm for 15 min and the cumulative fluorescence intensity was measured in the supernatant solution using a microplate reader with an excitation/emission wavelength of 490/528 nm.

To evaluate •OH generation during the second and third day after the initiation of hydration, 25 mg of microgels were first incubated in 750 μL of PB (pH 7.4) for 24 and 48 h, respectively, at 37 °C (in the dark) with gentle agitation on a shaking plate. Then, 3 μL of HPF (20 μM) was added to the microgel suspension while protected from ambient light and incubated for another 24 h at 37 °C. The fluorescence intensity was measured following the same protocol mentioned above.

The ability for the microgels to repeatedly generate •OH was evaluated by hydrating 25 mg of microgels in 750 μL of PB (pH 7.4). 3 μL of HPF (20 μM) was added to the microgel suspension while protected from ambient light and incubated for up to 12 h at room temperature with gentle agitation on a shaking plate. The fluorescence intensity was measured following the same protocol mentioned above. The microgels were washed in succession with acidic DI water (pH 3.5) and water (pH 7.4) and further incubated in PB and 3 μL of HPF (20 μM) for 12 h. This process was repeated 6 times to evaluate ability of the microgels to generate •OH after successive incubation in PB (pH 7.4).

Control experiments were performed by using Fe^{3+} ions or free HEM to generate •OH through the Fenton-like reaction. Either 50 μM Fe^{3+} or 3 μM HEM was added to 1-2 mM of H_2O_2 prepared by diluting 30% v/v H_2O_2 in DI water. The final reaction volume and pH were 1500 μL and 7.4, respectively. Methyl catechol (10 μM) was added to the Fe^{3+} solution as a reducing agent [31] in the absence of DMA-containing microgels. 25 mg of DMA or HEAA microgels were hydrated in 1500 μL of PB (pH 7.4) which contained 3 μM HEM or 1 mM Fe^{3+} aqueous solution. Finally, 10 μM HPF was added to the solutions and incubated for up to 24 h at 37 °C (in the dark) with gentle agitation on a shaking plate. The fluorescence intensity was measured following the same protocol mentioned above. The experiment was conducted in a triplet, and the results are reported as mean ± SD.

2.6. Organic dye degradation

25 mg of microgels were hydrated in 1500 μL of MG or OII solutions. MG and OII solutions were prepared by diluting a 1 mM stock solution of the dye in DI water into 20 μM solutions using PBS (pH 7.4). The microgel suspension was incubated for up to 24 h at 37 °C with gentle agitation on a shaking plate. Microgels were condensed by centrifugation at 8000 rpm for 15 min, and the concentration of the dye in the supernatant solution was determined using UV-vis (PerkinElmer Lambda35) at the wavelength of 617 nm and 484 nm for MG and OII, respectively. A series of solutions containing 0–20 μM of the dye was used to prepare a standard curve (Figure S2). The experiment was conducted in a triplet, and the results are reported as mean ± SD.

2.7. Antibacterial activity of microgels

The antibacterial activity of the microgels was evaluated using *S. epi* and *E. coli* while following published protocol with minor modifications.[32] A colony of the bacteria grown on an agar plate was used to inoculate 5 mL TSB in a sterile 50 mL Falcon tube. The bacteria culture was incubated at 37 ˚C on a shaking plate (100 rpm) for 20-24 h. The bacteria culture was then diluted using sterile PBS (pH 7.4) to 10^6 and 10^7 CFU/mL concentrations. 25 mg of ethylene oxide-sterilized microgels were equilibrated with 225 μL of sterile PBS (pH 7.4) and 500 μL of bacteria suspension was added. Each well was sealed with parafilm. The microgel and bacteria mixture was incubated at 37 °C for 24 h with gentle agitation on a shaking plate (100 rpm). At a given time point, a 10 μL loop was immersed into the bacteria solution without touching the precipitated microgels and streaked onto an agar plate. Agar plates were further incubated at 37 °C for 24-48 h. Colonies formed on the agar plates were photographed and counted using ImageJ. The relative colony number was calculated using the following equation: [33]

$$Relative\ Colony\ Number\ \% = \frac{N_m}{N_p} \times 100\%$$

where N_m is the number of colonies formed from the bacteria exposed to the microgels and N_p is the number of colonies formed from the bacteria exposed to PBS without microgel.

Morphology of both *S. epi* and *E. coli,* before and after exposure to the microgels, were imaged using FESEM (Hitachi S-4700). 25 mg of ethylene oxide-sterilized microgels were equilibrated with 225 µL of sterile PBS (pH 7.4) and mixed with 500 µL of bacteria suspension (10^7 CFU/mL). The mixture was incubated at 37 °C for 6 h with gentle agitation on a shaking plate (100 rpm). The microgel and bacterial mixture were centrifuged at 3500 rpm for 10 min, washed with PBS, and fixed with 2.5% glutaraldehyde solution overnight at 4 °C. Collected bacteria and microgel pellet washed with PBS and dehydrated through successive treatments by 30%, 50%, 70%, 80%, 90%, 95%, and 100% ethanol for 30 min during each treatment. Finally, the pellet was lyophilized overnight.

2.8. Antiviral properties of the microgels

PPV and BVDV were used to evaluate the viricidal activity of the microgels following previously published protocols.[19] 25 mg of ethylene oxide-sterilized microgels were hydrated by 225 µL of sterile PBS (pH 7.4) and, 500 µL of log 6 MTT_{50}/mL PPV or BVDV in PBS (pH 7.4) was added. The microgel mixture was incubated in a 5% CO_2 humidified incubator at 37 °C for up to 36 h. At given time points, the supernatants containing the treated virus were separated from the microgel by centrifugation at 6000 rpm for 5 min by a Sovall ST16R centrifuge (Thermo Scientific, Pittsburg, PA). The microgel-free supernatant was used to infect the indicator cells (PK-13 and BT-1 for PPV and BVDV, respectively). The virus was titrated using a colorimetric cell viability assay, the MTT assay, as described previously.[34] Briefly, cells for each virus (PK-13 cells with the density of $8x10^4$ cells/mL and BT cells with the density of 25 $x10^4$ cells/mL) were seeded in 96-well plates for 24 h to form a monolayer of cells. 25 µL of virus supernatant was added to the wells in quadruplicate, with a serial dilution of 1:5 across the plate. After 5 days, 5 mg/mL MTT solution (in PBS, pH 7.2) was incorporated into the wells for 4 h, followed by the addition of a stabilizing agent (10% SDS, pH 2) for another 24 h. The absorbance was measured at 550 nm using a Synergy Mx microplate reader (BioTek, Winoski,VT). The 50% infectious dose (MTT_{50}) of the virus was determined by measuring 50% uninfectious cell absorbance. Log reduction values (LRV) were calculated using the following equation:[35]

$$LRV = -\log\left(\frac{C_i}{C_f}\right)$$

where C_i is the initial concentration, and C_f is the final concentration.

An FEI 200kV Titan Themis STEM was used to image the virus particles while operating at 80 kV. Microgels were incubated with PPB for 36 h as described about and removed through centrifugation at 6000 rpm for 5 min by a Sovall ST16R centrifuge. The virus in the supernatant was fixed in 7.4 v/v% glutaraldehyde for 1 hour. The virus was deposited on a plasma-treated carbon type-B 300 mesh copper TEM grid (Ted Pella catalog #01813) and allowed to rest for 2-3 min to ensure proper attachment. The grid was then rinsed with nanopure water and negatively stained with a heavy metal salt in water (2 w/v% uranyl acetate in nanopure water) for 2 minutes. Finally, the grid was rinsed with nanopore water and dried in a desiccator for up to 48 h before imaging.

2.9. Microgels mesh size calculation

The mesh size (ξ) of microgels were calculated using the following equation:[36]

$$\xi = \nu_s^{-1/3}\left(\frac{2C_n\bar{M}_C}{M_n}\right)^{1/2} l$$

where υ_s is the volume fraction of the microgel in swollen state. C_n is the Flory characteristic ratio of polyHEAA, which was substituted by C_n of polyvinyl alcohol (8.3) [37] due to their similar hydroxyl functional group.[36] $\bar{M}_C$ and M_n are the average molecular weight of polymer between crosslinks, and the molecular weight of the repeating unit (115 Da for HEAA), respectively. l is the bond length along the polymer chain (1.54 Å for vinyl polymers). υ_s was calculated using the equation below:[38]

$$\nu_s = \frac{V_d}{V_s}$$

where V_d and V_s are the volume of the died and swollen microgels, respectively. Flory-Rehner equation was used to calculate $\bar{M}_C$:[39]

$$\bar{M}_C = -\frac{\rho_P V_{H_2O}(\nu_s^{1/3} - \nu_s/2)}{ln(1-\nu_s) + \nu_s + \chi\nu_s^2}$$

where ρ_P is the polymer density (1.31 g/cm^3 for polyHEAA),[40] V_{H2O} is the molar volume of water (18.1 cm^3/mol), and χ is the Flory-Huggins parameter for polyHEAA and water (0.5 when fully hydrated).[41]

2.10. Statistical analysis

Statistical analysis was performed using SigmaPlot. One-way analysis of variance (ANOVA) with the Tukey method for comparing means of multiple groups.

3. Results and discussion

3.1. Preparation of microgel functionalized with both HEM and Catechol

Microgels were prepared in a two-steps process. During the first step, microgels were prepared by photoinitiated polymerization of 10 mol% of DMA, HEAA (a hydrophilic monomer), APMA (an $–NH_2$ containing monomer) and up to 10 mol% METAC (cationic monomer), in an emulsion. In the second step, $–NH_2$ in APMA-functionalized microgels were further coupled to the carboxyl groups in HEM through carbodiimide chemistry. In

this design, DMA contains a catechol moiety that can autoxidize to generate H_2O_2 in a neutral pH solution and H_2O_2 can be further decomposed to $^{\bullet}OH$ in the presence of HEM through the Fenton-like reaction. The microgels were also functionalized with hydrophilic METAC, consisting of a positively charged nitrogen atom quaternary ammonium ions. METAC demonstrated antibacterial activity and the ability to interact with the negatively charged bacteria membrane.[24]

FTIR spectra of DMA-containing microgels exhibited the characteristic peaks for catechol at 1524 cm^{-1} and 1113 cm^{-1} associated with benzene ring stretching and phenol –OH groups, respectively (Figure S3).[19] For METAC-modified microgels a new peak appeared at 947 cm^{-1}, which corresponded to the quaternary ammonium functional group.[42] Incorporating HEM resulted in a new peak at 1020 cm^{-1}, which corresponded to the adsorbed O_2 on the Fe–OH moiety found in HEM.[43] However, free HEM exhibited this peak at 1040 cm^{-1} (Figure S3D). This peak is slightly shifted for HEM that is coupled to the microgel, potentially due to π–π interaction and hydrogen bonding between –OH groups on HEM and catechol.[43]

For HEM-modified microgels, the presence of Fe ions was confirmed by element mapping analysis performed by STEM-EDX on the crushed microgels (Figure S4). The HEM-modified microgels showed multiple regions in the crushed particles which contained Fe ions. The microgels with higher HEM reaction time demonstrated higher Fe ions distribution in their element mapping analysis. DMA-HEM-1h and DMA-METAC-HEM-1h showed the lowest Fe ion distribution when compared to other microgel formulations in their respective series. No Fe was detected from the microgels without HEM functionalities (i.e., DMA-m and DMA-METAC microgels). The residual mass after thermal decomposition was determined using TGA (Figure S5). Free HEM was highly stable, with over 60 wt% remained after heating to 700 °C. This is in agreement with previously published data for hemin, an Fe^{3+}-protoporphyrin with a chloride ion as the coordinating ion instead of hydroxide in HEM, where over 60 wt% remaining after heating to 800 °C.[44]

Thermal decomposition of HEM-functionalized microgels demonstrated that the residual mass increased with increasing reaction time with HEM. This indicated that a higher amount of HEM was coupled with the microgels when microgels functionalized with HEM longer (Table S1). For the longest reaction time of 24 h, the residual mass was around 13.5 and 11.5 wt% for DMA-HEM-24h and DMA-METAC-HEM-24h, respectively, with Fe content estimated to be 1.57 and 1.87 wt%, respectively. These microgels also appeared darker in color due to higher HEM content when compared to HEM-free samples and microgels with shorter reaction time (Figure S6). Theoretically, HEM can account for a maximum of 5 wt% based on the amount of APMA used during microgel preparation. The higher residual mass determined by TGA was potentially due to the formation of more stable compounds such as hemozoin (β-hematin) when HEM was heated to an elevated temperature.[44] Similar observation was reported when heating HEM-tethered polymer to a temperature of 700 °C.[45]

FESEM images indicated that the dried microgels were spherical in shape with an average diameter of around 9 µm (Figure S7 and Table S2) Functionalizing microgels with HEM did not affect the shape of the dried microgels. However, the average diameter of the dried HEM-functionalized microgels was increased to around 10-12 µm regardless of formulation. The size of the microgels increased after hydrating in PBS (pH 7.4) and the microgel retained the spherical shape. When the microgels were equilibrated in PBS, the particle size increased by 1.5-2 fold. Generally, microgels containing hydrophilic and charged METAC swelled more when compared to their METAC-free counterparts, potentially due to electrostatic repulsion. Zeta potential analysis indicated that DMA-METAC to be positively charged (33.1±0.6 mV, Table S3). Additionally, the swelling ratio decreased with increasing HEM-functionalization reaction time, due to the highly hydrophobic nature of the HEM functionalities.[46] For example, DMA-HEM-24h and DMA-METAC-HEM-24h exhibited the lowest swelling ration amongst all the fabricated microgels.

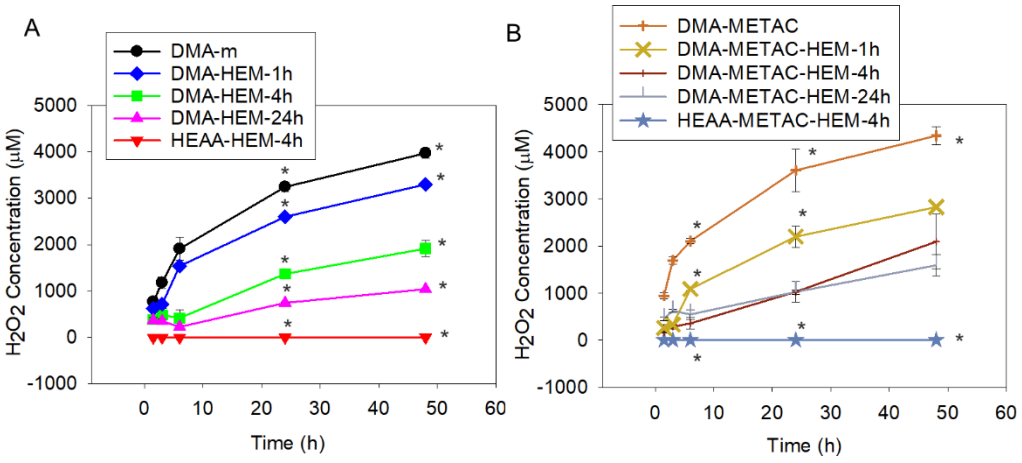

Figure 2. H_2O_2 generation from microgels without (A) and with (B) positively charged monomer, METAC. * $p < 0.05$ when compared to the other microgels at the same time point.

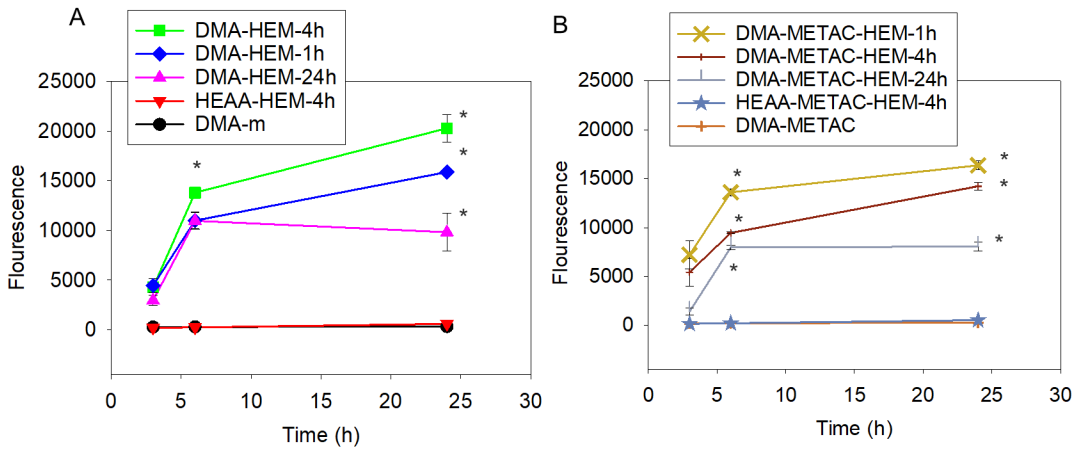

Figure 3. ˙OH detection using HPF probe from microgels without (A) and with (B) positively charged monomer, METAC. * $p < 0.05$ when compared to the other microgels at the same time point.

3.2. ROS generation from microgels

Microgels were hydrated in PBS (pH 7.4) and incubated at 37 °C, and the effect of HEM functionalization and METAC incorporation on the release of H_2O_2 and ˙OH was determined. Upon hydration, DMA-m microgel started to generate H_2O_2 and reached a maximum of 4000 µM of H_2O_2 after 48 h (Figure 2). Incorporation of METAC (e.g., DMA-METAC) increased the maximum release of H_2O_2 to 4500 µM. Additionally, H_2O_2 generation per catechol concentration, was significantly higher when compared with DMA-m microgels without METAC (Figure S8). METAC is cationic and likely increased the local pH due to its basic nature to promote catechol oxidation, resulting in higher H_2O_2 generation.[47] Incorporation of HEM significantly reduced the amount of H_2O_2 released from these microgels. Additionally, H_2O_2 concentration decreased with increasing content of HEM. DMA-HEM-24h and DMA-METAC-HEM-24h released a maximum of around 1000 µM within 48 h of incubation, a 4 fold reduction from HEM-free DMA microgels. This reduction in the amount of released H_2O_2 suggests that H_2O_2 was likely decomposed to ˙OH through the Fenton-like reaction in the presence of HEM. However, the hydrophobic nature of HEM also affected the H_2O_2 generation by the catechol due to reduced swelling, which restricted liquid exchange between the microgel and the surrounding medium.

The amount of ˙OH generated by the microgels was detected using HPF, an autoxidation-resistant fluorescence probe with the ability to reliably and selectively detect ˙OH.[48] Only microgels that contained both DMA and HEM generated ˙OH (Figure 3), indicating that both moieties are required for ˙OH generation. Fluorescence intensity increased over time and both DMA-HEM-4h and DMA-METAC-HEM-1h exhibited the highest fluorescence intensity values (17000-20000) when compared to other microgel formulations in their respective series. Although incorporation of METAC increased H_2O_2 release, it resulted in lower ˙OH generation when compared to the corresponding DMA-containing microgels without METAC. On the other hand, microgels with the highest HEM content (e.g., DMA-HEM-24h and DMA-METAC-HEM-24h) exhibited the lowest fluorescence intensity. The ratio of H_2O_2 to total Fe ions was reported to have a significant effect on ˙OH generation rate through the Fenton reaction.[28] Due to the hydrophobic nature of HEM, elevated HEM content restricted microgel swelling and likely affected catechol oxidation and H_2O_2 generation. As such, a balance of H_2O_2 generation and HEM content is required to maximize ˙OH generation. Regardless of formulation, HPF intensity values for the microgels were significantly higher when compared to a mixture of free HEM and 1-2 mM of H_2O_2 (Figure S9).

Microgels continue to generate ˙OH for up to 72 h (Figure S10). However, ˙OH generation occurred mostly in the first 24 h and significantly decreased over time. To determine if the microgels could be repeatedly activated to generate ˙OH, DMA- and HEM-containing microgels were repeatedly incubated in PB (pH 7.4) at room temperature for 12 h and washed with acidic DI water (pH 3.5), at the end of each incubation cycle (Figure S11). These microgels demonstrated the ability to be repeatedly activated to generate ˙OH during the first 4 cycles, with fluorescence intensity value of 10,000 – 15,000. However, the fluorescence intensity reduced with each subsequent cycle. This indicated that the microgel is reversible but has limited reversibility, possibly due to irreversible oxidative crosslinking of catechol through repeated oxidation.

A series of control experiments was performed to confirm the need to functionalize both catechol and HEM into a single microgel system. HPF fluorescence intensity detected by mixing DMA-m microgel with free HEM was around 10 times lower (Figure S9) when compared to the HEM-immobilized microgels (e.g., DMA-HEM-4h from Figure 3). This can be due to the direct interaction between free HEM and catechol, resulting in the formation of phenoxyl radicals in the presence of H_2O_2 and the heterolytic rupture of H_2O_2 as opposed to generating ˙OH.[9] Immobilization of HEM on the surface of the microgel prevented the direct interaction between catechol and HEM, which significantly enhanced ˙OH generation. Additionally, mixing DMA-m microgel with Fe^{3+} ions did not generate measurable amounts of HPF, even though H_2O_2 generation decreased (Figure S12). This is potentially due to the formation of catechol-Fe^{3+} ion complexation.[49] The stability of the complex at a physiological pH likely prevented Fenton reaction. Recently,

metal ion and nanoparticles were reported to induce catechol oxidation and production of singlet oxygen instead of •OH.[50, 51] Finally, neither H_2O_2 nor •OH was detected from HEAA microgels functionalized with HEM but without DMA (Figure 3). This indicated that catechol autoxidation is the source for H_2O_2 generation that is needed for the subsequent conversion to •OH.

3.3. Dye degradation experiments

OII and MG are commonly used in the manufacturing of food, paper, and textile.[52] However, these dyes are toxic and need to be removed from the environment. Decolorization and removal of these dyes through the Fenton-like reaction and •OH generation have been reported before,[53] and these dyes serve as good candidates for studying the ability of the microgels to degrade organic dyes. For example, more than 90% of MG and OII (10μM) were degraded through the conventional Fenton reaction using 2 mM H_2O_2 and 0.1 mM Fe ions at acidic pH values.[53] In another study, around 60% of MG was removed from the solution within 10 min using the electro-Fenton process at physiological pH.[54] The •OH generated from HEM-incorporated microgels (i.e., DMA-HEM-4h and DMA-METAC-HEM-4h) were able to degrade both OII and MG dyes successfully and reduced their amount to less than 20 and 5%, respectively (Figure 4).

The control microgels that contained only DMA or HEM also exhibited a relatively smaller amount of dye removal, potentially through the absorption of the dyes into the microgel network. In particular, microgels modified with only DMA demonstrated higher amount of dye reduction (60-40% for OII, and 8-13% for MG) when compared to HEM-modified microgels (more than 90% for OII, and 20-23% for MG, respectively). This enhanced removal is potentially due to the π-π interaction between the aromatic structures of the dyes and catechol.[55] Although the control microgels exhibited the ability to remove organic dyes from solutions, the •OH-generating microgels (DMA-HEM-4h and DMA-METAC-HEM-4h) still demonstrated a significantly higher dye removal capability over a 24 h period.

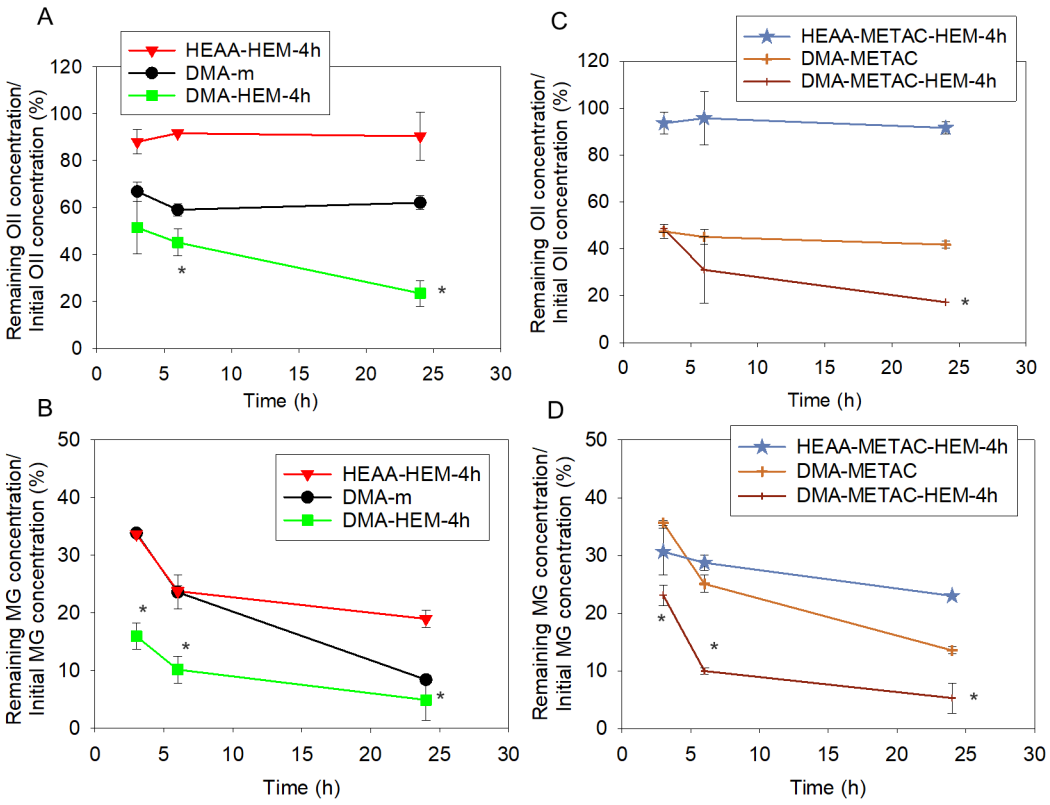

Figure 4. OII and MG degradation using DMA-m, HEAA-HEM-4h, DMA-HEM-4h (A, and B, respectively), and DMA-METAC, HEAA-METAC-HEM-4h and DMA-METAC-HEM-4h (C, and D, respectively) through the Fenton-like reaction. The starting dye concentration was 20 μM . * $p < 0.05$ when compared to the other microgels at the same time point.

3.4. Antibacterial activity of microgels

The antibacterial properties of microgels were investigated using both gram-positive (*S. epi*) and gram-negative (*E. coli*) bacteria at concentrations of 10^6 and 10^7 CFU/mL (Figures 5, 6, and S13-S16). The number of colonies formed over time reduced for both bacteria strains exposed to microgels modified with both HEM and DMA and no colony formed after 24 h of incubation. These microgels demonstrated more effective antimicrobial property when compared to catechol-functionalized microgels without HEM functionalities that release H_2O_2 (Figure S17), which were previously only able to demonstrate antimicrobial property against lower bacteria concentration of 10^5 CFU/mL.[19] Both bacteria strains cultured with HEM-incorporated microgels without DMA functionalities replicated rapidly overtime (Figures S13-16 f-o), indicating that •OH generation is the main antibacterial agent in our microgel system.

Microgels functionalized with METAC demonstrated a significantly faster reduction in the relative colony number when compared to microgels that did not contain METAC. Relative colony number of *E. coli* exposed to DMA-METAC-HEM-4h dropped to around 1% within 5 to 8 h. However, it took DMA-HEM-4h significantly longer to reach the similar level of reduction (8 and 24 h for *E. coli* with initial concentrations of 10^6 and 10^7 CFU/mL, respectively). Similarly, for *S. epi* with initial concentrations of 10^6 and 10^7 CFU/mL, the relative colony number decreased to the average of 14 and 21%, respectively, within 1h of exposure to DMA-METAC-HEM-4h. While more than 50% of *S. epi* were still alive after exposure to DMA-HEM-4h for 1 h.

The antibacterial activity of polymers functionalized with METAC was broadly investigated before.[56] The positively charged METAC can attract the negatively charged bacteria, diffuse through their cell wall, and disrupt their cytoplasmic membrane leading to cell death. Both bacteria used in this experiment possess a net negative charge on their cell wall, with *S. epi* demonstrated a greater net negative charge than *E. coli*.[57] However, the bacteria exposed to HEAA-METAC-HEM-4h (control microgel without DMA) was ineffective against both bacteria, indicating that having METAC alone was insufficient in killing the bacteria under our experimental conditions. Therefore, the synergetic effect of the released •OH and METAC functionalities was considered as the main reason for the potent antibacterial properties of this microgel system. •OH has an extremely short half-life (10^{-9} s) and rapidly decomposes to water and O_2 in an aqueous solution.[58] This is in great contrast with the more stable H_2O_2 with a half-life of 10^4-10^6 s.[59] The positively charged METAC attracted the negatively charged bacteria cells and enhanced the antibacterial effect of •OH-releasing microgels.

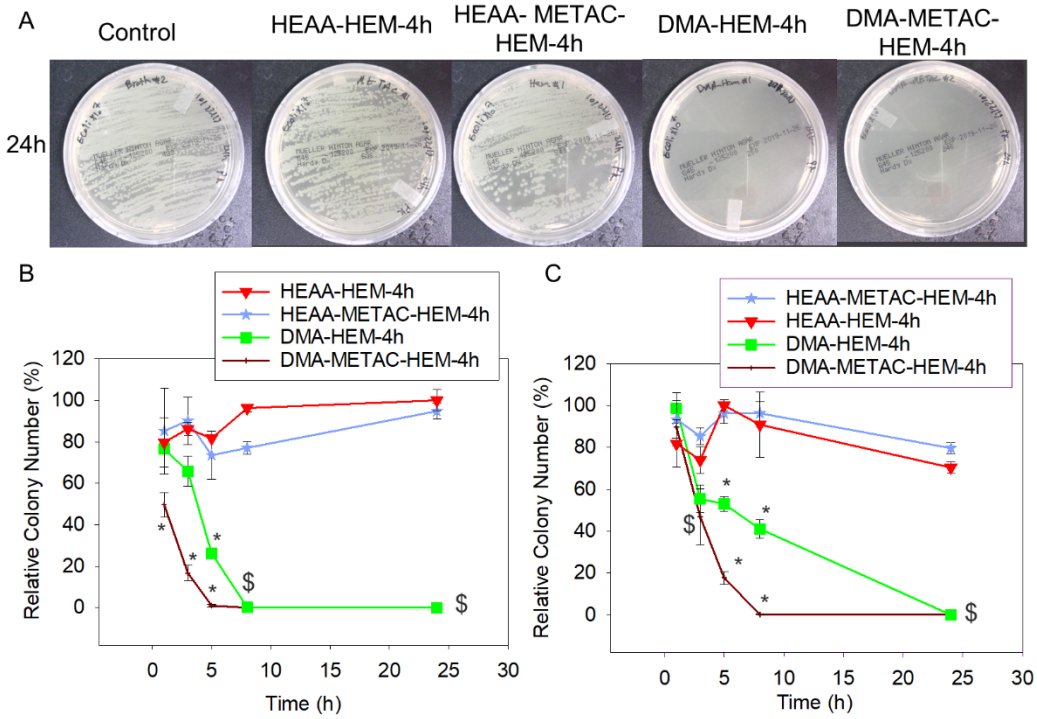

Figure 5. Photograph of the test plates with *E. coli* colonies (with initial concentration of 10^7 CFU/ml) exposed to DMA-HEM-4h, HEAA-HEM-4h, DMA-METAC-HEM-4h, HEAA-METAC-HEM-4h microgels and PBS (control) after 24h (A). Relative bacteria colony number for *E. coli* (with the initial concentration of 10^6 and 10^7 CFU/ml, B, and C respectively) incubated with the microgels. The relative colony number was normalized by the number of colonies formed by the bacteria not treated with microgels. * $p < 0.05$ when compared to the other microgels at the same time point. $ $p < 0.05$ when compared to the controls (HEAA-HEM-4h and HEAA-METAC-HEM-4h) at the same time point. The data points associated with the controls were not statistically significant over time.

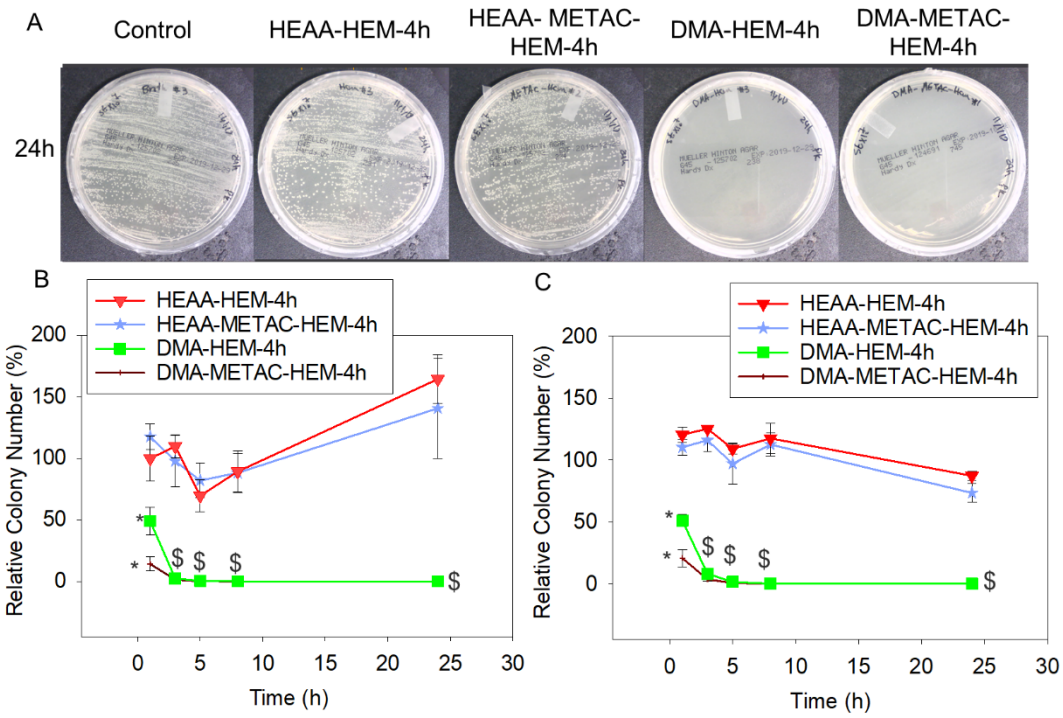

Figure 6. Photograph of the test plates with *S. epi* colonies (initial concentration of 10^7 CFU/ml) exposed to DMA-HEM-4h, HEAA-HEM-4h, DMA-METAC-HEM-4h, HEAA-METAC-HEM-4h microgels and PBS (control) after 24h (A). Relative bacteria colony number for *S. epi* (with the initial concentration of 10^6 and 10^7 CFU/ml, B, and C respectively) incubated with the microgels. The relative colony number was normalized by the number of colonies formed by the bacteria not treated with microgels. * $p < 0.05$ when compared to the other microgels at the same time point. $ $p < 0.001$ when compared to the controls (HEAA-HEM-4h and HEAA-METAC-HEM-4h) at the same time point. The early time points data (within the first 8 h) associated with the controls were not statistically significant.

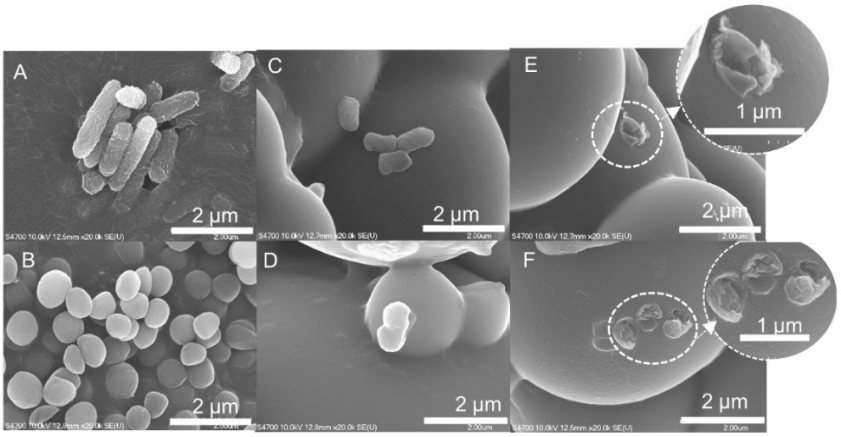

Figure 7. FESEM images of *E. coli* (A, C, and E) and *S. epi* (B, D, and F) exposed to PBS (A and B), DMA-m microgels (C and D) and DMA-METAC-HEM-4h microgels (E and F). The initial concentration of bacteria was 10^7 CFU/ml. The inset images in E and F show the magnified images of the distorted bacterial cell membrane after exposure to DMA-METAC-HEM-4h microgels.

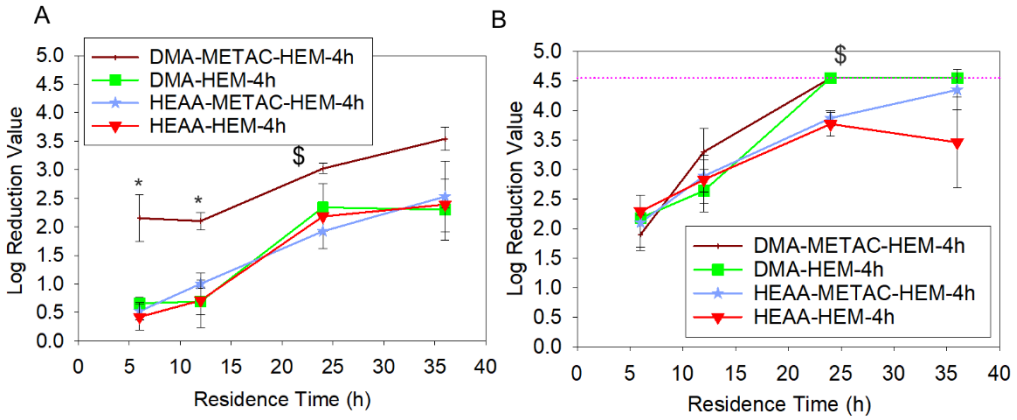

Figure 8. Log reduction value for PPV (A) and BVDV (B) exposed to DMA-HEM-4h, HEAA-HEM-4h, DMA-METAC-HEM-4h, and HEAA-METAC-HEM-4h microgels with a starting viral titer of 6 log. * $p < 0.05$ when compared to the other microgels at the same time point. $ $p < 0.05$ when compared to the controls (HEAA-HEM-4h and DMA-METAC-HEM-4h) at the same time point. Pink dashed line represents the detection limit.

DMA-METAC-HEM-4h microgels demonstrated stronger antibacterial activities within a similar time period when compared to other materials that induce similar Fenton-like reactions. A cinnamaldehyde-containing micelle encapsulated Fe-containing ferrocene could induce the generation of H_2O_2 in bacteria cells, which further converted to •OH through the Fenton-like reaction.[60] The survival rate of *E. coli* (with initial concentrations of 10^5 CFU/mL) exposed to this polymeric material dropped to less than 20% within 1 h. A nano-enzyme hydrogel containing copper oxide nanoparticles and glucose oxide demonstrated •OH generation during the free-radical polymerization process.[61] Growth of *E. coli* (with the initial concentration of 10^8 CFU/mL) was inhibited within 7 h of exposure to the mixture of the nano-enzyme and glucose oxide.

Morphological changes of both bacteria strains before and after exposure to H_2O_2-generating DMA-m and •OH-generating DMA-METAC-HEM-4h microgels were investigated using FESEM (Figure 7). Both untreated bacteria cells were intact with a well-maintained cell wall and well-defined morphology. The bacteria exposed to the DMA-m microgels indicated minor morphological deformations. *E. coli* cells appeared smaller in size when compared to the untreated cells, suggesting the leakage of the cell's interior content. Both strains of the bacteria exposed to the DMA-METAC-HEM-4h microgels completely lost their morphological, structural, and cellular integrity, which resulted in cellular lysis. *S. epi* cells were completely decomposed, and only the trace of the cells' membrane was apparent. These results were in line with the previous published SEM images obtained for H_2O_2- and •OH-treated bacteria.[62, 63]

3.5. Antiviral properties of microgels

The viricidal activity of microgels was investigated against both non-enveloped PPV and the enveloped BVDV with a starting viral titer of 6 $\log_{10}$MTT/mL (Figure 8). Only DMA-METAC-HEM-4h microgels were able to reduce the PPV titer value by nearly 3.5 LRV after 36 h of incubation. This corresponds to a 99.97% reduction in infectivity, which is significantly higher than that of catechol-functionalized microgels, which had a reduction of 3 LRV.[19] PPV is a highly chemical resistant virus and challenging to inactivate.[64] However, a 3.5 LRV is approaching the 4 log reduction limit approved by the EPA and FDA for a virus inactivation method. Additionally, both HEM-incorporated microgels containing DMA (DMA-HEM-4h and DMA-METAC-HEM-4h) reduced the BVDV titer value by 4.5 LRV (99.997% reduced infectivity) within 24 h. After 24 h, the values reached the MTT detection limitation. This indicated that the cell viability was higher than what the assay can be used to quantify the viral concentration, due to an extremely low viral titer. These results are consistent with the previous findings that the enveloped virus was more susceptible to the destructive effect of the •OH released from a TiO_2/UV system.[65] Unlike the bacteria treated with the microgels, there was no apparent morphological change in PPV after treatment with either H_2O_2-releasing DMA-m or •OH-releasing DMA-METAC-HEM-4h (Figure S4). Additionally, the viral particle size remained around 20 nm regardless of treatment (Table S4), which is in agreement with the reported size of PPV (18–26 nm).[25] This indicated that the antiviral mechanism differed from that of the antimicrobial mechanism. Virus inactivation by •OH is believed to involve the genomic damage.[66] •OH initiates abstraction of nucleosides hydrogen atoms which leads to carbon radical's formation and eventually single- or double-strand breaks.

DMA-HEM-4h microgel did not inactivate PPV as efficiently as DMA-METAC-HEM-4h, despite releasing the highest concentration of •OH among all the fabricated microgels (Figure 3). This can be attributed to the short half-life of •OH [67] and the lack of METAC functionalities to attract the negatively charged viruses toward the microgel (Figure 9). Both PPV and BVDV have a negative net surface charge under physiological pH conditions.[25] Additionally, the presence of cation also synergistically promoted interfacial binding capabilities of catechol,[68] potentially facilitated their removal from solution.

HEM-incorporated HEAA microgels that did not contain DMA also reduced PPV and BVDV titer value by over 2 and 4 LRV, respectively, after 36 h (Figure 8). Previously, diffusion of the viruses into the microgel network was reported as the possible mechanism for the reduction in infectivity of the viruses exposed to HEAA microgels.[19] However, the mesh sizes of HEM-modified microgels (Table S5) were smaller (2-15 nm) when compared to the reported size of PPV and BVDV (40–60 nm).[25]

The reduction in virus titer values is likely associated with the Fe-containing HEM functionalities. Heme, an Fe^{2+}-protoporphyrin with chloride ion as the coordinating ion, demonstrated similar ability to inactivate enveloped Dengue and yellow fever viruses.[69] The Fe ions and the tetrapyrrolic ring structure were reported as the main reason for this viricidal activity.

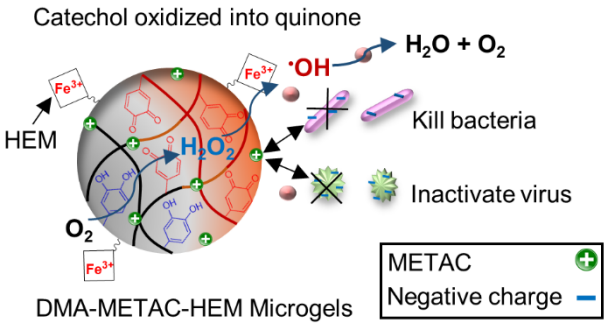

Figure 9. Schematic representation of DMA-METAC-HEM microgel's activation, and •OH generation through the Fenton-like reaction. •OH is a potent ROS with a very short half-life. The microgels were functionalized with catanionic species (positive charges), which attracts negatively charged organisms. The synergetic effect of released •OH and METAC functionalities significantly enhances the antipathogenic and dye removal activities.

Taken together, we combined catechol and HEM to create a single microgel system that can release a highly reactive oxidant, •OH. In this design, catechol autoxidizes in physiological pH to generate H_2O_2, while HEM converts the generated H_2O_2 into •OH using a Fenton-like reaction. Protoporphyrin derivatives, including HEM, are very stable ligands due to their cyclically constrained constriction.[70] These tetradentate ligands, which use four nitrogen atoms to bind to one Fe ion in coordination complexes, are more stable when compared to bidentate and tridentate ligands like catechol. This prevented direct interaction between catechol and Fe ions to form a complex that does not promote Fenton reaction. Fenton and Fenton-like reactions were typically carried out in acidic conditions with the pH around 3-4 to avoid the precipitation of Fe in the form of hydroxide.[11] HEM stayed reactive in physiological conditions, which minimizes the need to adjust the pH to an acidic values for an efficient Fenton reaction.[9] Due to the extremely short half-life of •OH, the residual toxicity is negligible.[10] In fact, the addition of positively charged METAC was required to enhance the antibacterial and antiviral property through electrostatic interaction between the microgel and the negatively charged pathogens.

The reported microgels do not contain a reservoir for releasing the highly reactive •OH. These microgels are only activated to generate ROS when they are hydrated in an aqueous solution. Because the microgel itself does not contain any ROS, it is less hazardous to store and transport when compared to other sources of the reactive ROS. Additionally, these microgels can generate •OH without the need for bulky and expensive equipment or an external source of H_2O_2 to initiate Fenton reactions.[11, 12, 71] These microgels can potentially function as a lightweight and portable source for on-demand generation of •OH for wastewater purification and antipathogenic applications.

This work is the first demonstration of a microgel system that can be activated to generate •OH with simple hydration. However, microgel formulations may need to be optimized to enhance its ROS generation capability. Due to the microgel's ability to swell, it likely reached the capacity in terms of the concentration of microgels that could be added in the current testing methods. As such, to further increase the generation of •OH, there is a need to increase DMA content as well as balance its ratio with the content of HEM.

4. Conclusion

Microgels were successfully functionalized with both HEM and catechol. When the microgels were hydrated in a solution with physiological pH, catechol converted O_2 into H_2O_2 through autoxidation and the generated H_2O_2 were decomposed to •OH through the Fenton-like reaction by HEM. The •OH-releasing microgels were able to degrade organic dyes, including OII and MG, and reduced their amount to less than 20 and 5%, respectively, in 24 h. Additionally, these microgels were antibacterial against both gram-positive (*S. epi*) and gram-negative (*E. coli*) bacteria with a starting concentration of 10^6-10^7 CFU/mL and antiviral against both non-enveloped (PPV) and the enveloped (BVDV) viruses. The incorporation of positively charged METAC significantly enhanced the antibacterial and antiviral activities of the microgels through electrostatic interaction between the microgel and the negatively charged pathogens.

ASSOCIATED CONTENT

Supporting Information.
Schematic illustration of HEM- and DMA-containing microgel's preparation, standard curves for MG and OII dyes, ATR-FTIR spectra, STEM-EDX images, and TGA of microgels, effect of HEM-functionalization reaction time on the color of the microgels, FESEM and phase contrast microscopy images and swelling ratios, Zeta potential analysis, H_2O_2 generation normalized to the catechol concentration, additional •OH detection using HPF, Photograph of the test plates with *E. coli* and *S. epi* colonies, additional relative bacteria colony number for *E. coli* and *S. epi* incubated with microgels, STEM images and size distribution of PPV, and the mesh size of microgels. This material is available free of charge via the Internet at http://pubs.acs.org.

AUTHOR INFORMATION

Corresponding Author

Bruce P. Lee-department of Biomedical Engineering, Michigan Technological University, Houghton, MI 49931, USA
Email: bplee@mtu.edu

Author Contributions

The manuscript was written through contributions of all authors. All authors have given approval to the final version of the manuscript.

Notes

The authors declare no competing financial interest.

ACKNOWLEDGMENT

The authors acknowledge funding from the National Institutes of Health under Award Nos. R15GM104846 (B.P.L), R15GM135875 (B.P.L), and R15GM112082 (R.M.R.), the Office of the Assistant

Secretary of Defense for Health Affairs through the Defense Medical Research and Development Program under Award No. W81XWH1810610 (B.P.L), the Office of Naval Research under Award No. N00014-16-1-2463 (B.P.L.), the National Science Foundation under Award No. DMR 2001076 (B.P.L.) and CBET 1451959 (C.L.H.), and the Mack Chair in Bioengineering (C.L.H.). P.K.F. and R.P. were supported in part by the Doctoral Finishing Fellowship provided by the Portage Health Foundation. A.T. was supported by the King-Chávez-Parks Future faculty fellowship. We thank Director Owen Mills and the Applied Chemical & Morphological Analysis Laboratory (ACMAL) at Michigan Technological University for the use of instruments and staff assistance. We thank Dr. Pinaki Mukherjee for running the STEM-EDX experiment. Electron microscopy facility is supported by NSF MRI 1429232.

ABBREVIATIONS

H_2O_2, hydrogen peroxide; •OH, hydroxyl radical; $O_2^{\cdot-}$, superoxide; HEM, hematin; DMA, dopamine methacrylamide; HEAA, N-Hydroxyethyl acrylamide; APMA, N-(3-Aminopropyl)methacrylamide hydrochloride; METAC, ([2-(methacryloyloxy)ethyl] trimethylammonium chloride; S. epi, Staphylococcus epidermidis; E. coli, Escherichia coli; PPV, Porcine parvovirus; BVDV, Bovine viral diarrhea virus; HEAA-m microgel, the microgels contain 0 mol% DMA ; HEAA-METAC microgels, the microgels contain 0 mol% DMA and 10 mol% METAC ; DMA-m microgel, the microgels contain 10 mol% DMA; DMA-METAC microgel, the microgels contain 10 mol% DMA and 10 mol% METAC; DMA-HEM-1 to 24h microgel, the microgels contain 10 mol% DMA which functionalized with HEM for 1 to 24 h; DMA-METAC-HEM-1 to 24h microgel, the microgels contain 10 mol% DMA and 10 mol% METAC which functionalized with HEM for 1 to 24 h; LRV, log reduction value.

REFERENCES

1. Winterbourn, C. C., Reconciling the chemistry and biology of reactive oxygen species. Nat. Chem. Biol 2008, 4, (5), 278-286.
2. Imlay, J. A., Iron-sulphur clusters and the problem with oxygen. Mol. Microbiol. 2006, 59, (4), 1073-1082.
3. Pignatello, J. J.; Oliveros, E.; MacKay, A., Advanced Oxidation Processes for Organic Contaminant Destruction Based on the Fenton Reaction and Related Chemistry. Crit. Rev. Environ. Sci. Technol. 2006, 36, (1), 1-84.
4. Buxton, G. V.; Greenstock, C. L.; Helman, W. P.; Ross, A. B., Critical review of rate constants for reactions of hydrated electrons, hydrogen atoms and hydroxyl radicals (· OH/· O− in aqueous solution. J. Phys. Chem. Ref. Data 1988, 17, (2), 513-886.
5. Imlay, J. A., Pathways of oxidative damage. Annu. Rev. Microbiol 2003, 57, (1), 395-418.
6. Bogdan, J.; Zarzyńska, J.; Pławińska-Czarnak, J., Comparison of Infectious Agents Susceptibility to Photocatalytic Effects of Nanosized Titanium and Zinc Oxides: A Practical Approach. Nanoscale Res. Lett. 2015, 10, (1), 309.
7. Kohanski, M. A.; Dwyer, D. J.; Hayete, B.; Lawrence, C. A.; Collins, J. J., A common mechanism of cellular death induced by bactericidal antibiotics. Cell 2007, 130, (5), 797-810.
8. Luong*, H. V.; Lin, H. K., Controlling the Fenton Reaction for Soil Remediation. Anal. Lett. 2000, 33, (14), 3051-3065.
9. Magario, I.; García Einschlag, F. S.; Rueda, E. H.; Zygadlo, J.; Ferreira, M. L., Mechanisms of radical generation in the removal of phenol derivatives and pigments using different Fe-based catalytic systems. J. Mol. Catal. A: Chem. 2012, 352, 1-20.
10. Nakamura, K.; Shirato, M.; Kanno, T.; Örtengren, U.; Lingström, P.; Niwano, Y., Antimicrobial activity of hydroxyl radicals generated by hydrogen peroxide photolysis against Streptococcus mutans biofilm. Int. J. Antimicrob. Agents 2016, 48, (4), 373-380.
11. Lee, H.; Lee, H.-J.; Seo, J.; Kim, H.-E.; Shin, Y. K.; Kim, J.-H.; Lee, C., Activation of Oxygen and Hydrogen Peroxide by Copper(II) Coupled with Hydroxylamine for Oxidation of Organic Contaminants. Environ. Sci. Technol. 2016, 50, (15), 8231-8238.
12. Klamerth, N.; Malato, S.; Agüera, A.; Fernández-Alba, A., Photo-Fenton and modified photo-Fenton at neutral pH for the treatment of emerging contaminants in wastewater treatment plant effluents: a comparison. Water Res. 2013, 47, (2), 833-840.
13. Sklari, S. D.; Plakas, K. V.; Petsi, P. N.; Zaspalis, V. T.; Karabelas, A. J., Toward the Development of a Novel Electro-Fenton System for Eliminating Toxic Organic Substances from Water. Part 2. Preparation, Characterization, and Evaluation of Iron-Impregnated Carbon Felts as Cathodic Electrodes. Ind. Eng. Chem. Res. 2015, 54, (7), 2059-2073.
14. Waite, J. H., Nature's underwater adhesive specialist. Int. J. Adhes. Adhes. 1987, 7, (1), 9-14.
15. McDowell, L. M.; Burzio, L. A.; Waite, J. H.; Schaefer, J., Rotational echo double resonance detection of cross-links formed in mussel byssus under high-flow stress. J. Biol. Chem. 1999, 274, (29), 20293-20295.
16. Meng, H.; Li, Y.; Faust, M.; Konst, S.; Lee, B. P., Hydrogen peroxide generation and biocompatibility of hydrogel-bound mussel adhesive moiety. Acta Biomater. 2015, 17, 160-169.
17. Mochizuki, M.; Yamazaki, S.-i.; Kano, K.; Ikeda, T., Kinetic analysis and mechanistic aspects of autoxidation of catechins. Biochim. Biophys. Acta 2002, 1569, (1), 35-44.
18. Kord Forooshani, P.; Lee, B. P., Recent approaches in designing bioadhesive materials inspired by mussel adhesive protein. J Polym Sci A Polym Chem 2017, 55, (1), 9-33.
19. Meng, H.; Forooshani, P. K.; Joshi, P. U.; Osborne, J.; Mi, X.; Meingast, C.; Pinnaratip, R.; Kelley, J.; Narkar, A.; He, W.; Frost, M. C.; Heldt, C. L.; Lee, B. P., Biomimetic recyclable microgels for on-demand generation of hydrogen peroxide and antipathogenic application. Acta Biomater. 2019, 83, 109-118.
20. Mustafa, H. S. I., Staphylococcus Aureus can Produce Catalase Enzyme when React with Human Wbcs as a Source of H2O2 Productions in Human Plasma or Serum in the Laboratory. J Med Microbiol Diagn 2014, 04, (04), 3.
21. Dunford, H. B., Heme peroxidases. Wiley-vch: 1999.
22. Nam, W.; Han, H. J.; Oh, S.-Y.; Lee, Y. J.; Choi, M.-H.; Han, S.-Y.; Kim, C.; Woo, S. K.; Shin, W., New Insights into the Mechanisms of O−O Bond Cleavage of Hydrogen Peroxide and tert-Alkyl Hydroperoxides by Iron(III) Porphyrin Complexes. J. Am. Chem. Soc. 2000, 122, (36), 8677-8684.
23. Kalyanaraman, B.; Mottley, C.; Mason, R. P., A direct electron spin resonance and spin-trapping investigation of peroxyl free radical formation by hematin/hydroperoxide systems. J. Biol. Chem. 1983, 258, (6), 3855-3858.
24. Nonaka, T.; Noda, E.; Kurihara, S., Graft copolymerization of vinyl monomers bearing positive charges or episulfide groups onto loofah fibers and their antibacterial activity. J. Appl. Polym. Sci. 2000, 77, (5), 1077-1086.
25. Mi, X.; Bromley, E. K.; Joshi, P. U.; Long, F.; Heldt, C. L., Virus Isoelectric Point Determination Using Single-Particle Chemical Force Microscopy. Langmuir 2020, 36, (1), 370-378.
26. Lee, H.; Lee, B. P.; Messersmith, P. B., A reversible wet/dry adhesive inspired by mussels and geckos. Nature 2007, 448, (7151), 338.

27. Sambrook, J.; Fritsch, E. F.; Maniatis, T., Molecular cloning: a laboratory manual. Cold spring harbor laboratory press: 1989.
28. Du, Y.; Zhou, M.; Lei, L., Role of the intermediates in the degradation of phenolic compounds by Fenton-like process. J. Hazard. Mater. 2006, 136, (3), 859-865.
29. Zhang, X.-Z.; Chu, C.-C., Fabrication and characterization of microgel-impregnated, thermosensitive PNIPAAm hydrogels. Polymer 2005, 46, (23), 9664-9673.
30. Clement, M. V.; Long, L. H.; Ramalingam, J.; Halliwell, B., The cytotoxicity of dopamine may be an artefact of cell culture. J. Neurochem. 2002, 81, (3), 414-421.
31. Iwahashi, H.; Morishita, H.; Ishii, T.; Sugata, R.; Kido, R., Enhancement by catechols of hydroxyl-radical formation in the presence of ferric ions and hydrogen peroxide. J. Biochem. 1989, 105, (3), 429-434.
32. Häntzschel, N.; Hund, R.-D.; Hund, H.; Schrinner, M.; Lück, C.; Pich, A., Hybrid Microgels with Antibacterial Properties. Macromol. Biosci. 2009, 9, (5), 444-449.
33. Vilčnik, A.; Jerman, I.; Šurca Vuk, A.; Koželj, M.; Orel, B.; Tomšič, B.; Simončič, B.; Kovač, J., Structural Properties and Antibacterial Effects of Hydrophobic and Oleophobic Sol−Gel Coatings for Cotton Fabrics. Langmuir 2009, 25, (10), 5869-5880.
34. Heldt, C. L.; Hernandez, R.; Mudiganti, U.; Gurgel, P. V.; Brown, D. T.; Carbonell, R. G., A colorimetric assay for viral agents that produce cytopathic effects. J. Virol. Methods 2006, 135, (1), 56-65.
35. Tafur, M. F.; Vijayaragavan, K. S.; Heldt, C. L., Reduction of porcine parvovirus infectivity in the presence of protecting osmolytes. Antiviral Res. 2013, 99, (1), 27-33.
36. Peppas, N.; Bures, P.; Leobandung, W.; Ichikawa, H., Hydrogels in pharmaceutical formulations. Eur. J. Pharm. Biopharm. 2000, 50, (1), 27-46.
37. Gudeman, L. F.; Peppas, N. A., Preparation and characterization of pH-sensitive, interpenetrating networks of poly (vinyl alcohol) and poly (acrylic acid). J. Appl. Polym. Sci. 1995, 55, (6), 919-928.
38. Andreopoulos, F. M.; Beckman, E. J.; Russell, A. J., Light-induced tailoring of PEG-hydrogel properties. Biomaterials 1998, 19, (15), 1343-1352.
39. Flory, P. J.; Rehner Jr, J., Statistical mechanics of cross-linked polymer networks I. Rubberlike elasticity. J. Chem. Phys 1943, 11, (11), 512-520.
40. Pandis, C.; Spanoudaki, A.; Kyritsis, A.; Pissis, P.; Hernández, J. C. R.; Gómez Ribelles, J. L.; Monleón Pradas, M., Water sorption characteristics of poly (2-hydroxyethyl acrylate)/silica nanocomposite hydrogels. J. Polym. Sci., Part B: Polym. Phys. 2011, 49, (9), 657-668.
41. Pradas, M. M.; Ribelles, J. G.; Aroca, A. S.; Ferrer, G. G.; Antón, J. S.; Pissis, P., Interaction between water and polymer chains in poly (hydroxyethyl acrylate) hydrogels. Colloid Polym. Sci. 2001, 279, (4), 323-330.
42. Wang, S.; Hou, Q.; Kong, F.; Fatehi, P., Production of cationic xylan–METAC copolymer as a flocculant for textile industry. Carbohydr. Polym. 2015, 124, 229-236.
43. Amreen, K.; Senthil Kumar, A., Highly Redox-Active Hematin-Functionalized Carbon Mesoporous Nanomaterial for Electrocatalytic Reduction Applications in Neutral Media. ACS Appl. Nano Mater. 2018, 1, (5), 2272-2283.
44. Slocik, J. M.; Drummy, L. F.; Dickerson, M. B.; Crouse, C. A.; Spowart, J. E.; Naik, R. R., Bioinspired High-Performance Energetic Materials Using Heme-Containing Crystals. Small 2015, 11, (29), 3539-3544.
45. Nagarajan, S.; Nagarajan, R.; Bruno, F.; Samuelson, L.; Kumar, J., Nagarajan, S., Nagarajan, R., Bruno, F., Samuelson, L. A. & Kumar, J. A stable biomimetic redox catalyst obtained by the enzyme catalyzed amidation of iron porphyrin. Green Chem. 11, 334-338. Green Chem. 2009, 11.
46. Vekilov, P. G.; Rimer, J. D.; Olafson, K. N.; Ketchum, M. A., Lipid or aqueous medium for hematin crystallization? CrystEngComm 2015, 17, (41), 7790-7800.
47. Narkar, A. R.; Kelley, J. D.; Pinnaratip, R.; Lee, B. P., Effect of Ionic Functional Groups on the Oxidation State and Interfacial Binding Property of Catechol-Based Adhesive. Biomacromolecules 2018, 19, (5), 1416-1424.
48. Setsukinai, K.-i.; Urano, Y.; Kakinuma, K.; Majima, H. J.; Nagano, T., Development of novel fluorescence probes that can reliably detect reactive oxygen species and distinguish specific species. J. Biol. Chem. 2003, 278, (5), 3170-3175.
49. Taylor, S. W.; Luther III, G. W.; Waite, J. H., Polarographic and spectrophotometric investigation of iron (III) complexation to 3, 4-dihydroxyphenylalanine-containing peptides and proteins from Mytilus edulis. Inorg. Chem. 1994, 33, (25), 5819-5824.
50. Yi, Q.; Ji, J.; Shen, B.; Dong, C.; Liu, J.; Zhang, J.; Xing, M., Singlet oxygen triggered by superoxide radicals in a molybdenum cocatalytic fenton reaction with enhanced REDOX activity in the environment. Environ. Sci. Technol. 2019, 53, (16), 9725-9733.
51. Zhang, Z.; He, X.; Zhou, C.; Reaume, M.; Wu, M.; Liu, B.; Lee, B. P., Iron Magnetic Nanoparticle-Induced ROS Generation from Catechol-Containing Microgel for Environmental and Biomedical Applications. ACS Appl. Mater. Interfaces 2020, 12, (19), 21210-21220.
52. Crini, G., Non-conventional low-cost adsorbents for dye removal: A review. Bioresour. Technol. 2006, 97, (9), 1061-1085.
53. Chen, F.; Ma, W.; He, J.; Zhao, J., Fenton Degradation of Malachite Green Catalyzed by Aromatic Additives. J. Phys. Chem. A 2002, 106, (41), 9485-9490.
54. Teymori, M.; Khorsandi, H.; Aghapour, A. A.; Jafari, S. J.; Maleki, R., Electro-Fenton method for the removal of Malachite Green: effect of operational parameters. Appl. Water Sci. 2019, 10, (1), 39.
55. Zhang, Z.; He, X.; Zhou, C.; Reaume, M.; Wu, M.; Liu, B.; Lee, B. P., Iron Magnetic Nanoparticle-Induced ROS Generation from Catechol-Containing Microgel for Environmental and Biomedical Applications. ACS Appl. Mater. Interfaces 2020.
56. Lu, G.; Wu, D.; Fu, R., Studies on the synthesis and antibacterial activities of polymeric quaternary ammonium salts from dimethylaminoethyl methacrylate. React. Funct. Polym. 2007, 67, (4), 355-366.
57. Dickson, J. S.; Koohmaraie, M., Cell surface charge characteristics and their relationship to bacterial attachment to meat surfaces. Appl. Environ. Microbiol. 1989, 55, (4), 832-836.
58. SIES, H., Strategies of antioxidant defense. Eur J Biochem 1993, 215, (2), 213-219.
59. Hydrogen Peroxide (20 to 40%); FMC Corporation: 2009.
60. Park, S. C.; Kim, N. H.; Yang, W.; Nah, J. W.; Jang, M. K.; Lee, D., Polymeric micellar nanoplatforms for Fenton reaction as a new class of antibacterial agents. J Control Release 2016, 221, 37-47.
61. Ye, Y.; Xiao, L.; He, B.; Zhang, Q.; Nie, T.; Yang, X.; Wu, D.; Cheng, H.; Li, P.; Wang, Q., Oxygen-tuned nanozyme polymerization for the preparation of hydrogels with printable and antibacterial properties. J. Mater. Chem. B 2017, 5, (7), 1518-1524.

62. Huang, T.; Sui, M.; Li, J., Inactivation of E. coli by nano-Cu/MWCNTs combined with hydrogen peroxide. Sci. Total Environ. 2017, 574, 818-828.
63. Dong, X.; Awak, M. A.; Tomlinson, N.; Tang, Y.; Sun, Y.-P.; Yang, L., Antibacterial effects of carbon dots in combination with other antimicrobial reagents. PloS one 2017, 12, (9), e0185324.
64. Muzyczka, N.; Berns, K., Parvoviridae: the viruses and their replication. Fields virology 2001, 2, 2327-2359.
65. Nakano, R.; Hara, M.; Ishiguro, H.; Yao, Y.; Ochiai, T.; Nakata, K.; Murakami, T.; Kajioka, J.; Sunada, K.; Hashimoto, K., Broad spectrum microbicidal activity of photocatalysis by TiO2. Catalysts 2013, 3, (1), 310-323.
66. Termini, J., Hydroperoxide-induced DNA damage and mutations. MUTAT RES-FUND MOL M 2000, 450, (1), 107-124.
67. Pryor, W. A., Oxy-radicals and related species: their formation, lifetimes, and reactions. Annu. Rev. Physiol. 1986, 48, (1), 657-667.
68. Rapp, M. V.; Maier, G. P.; Dobbs, H. A.; Higdon, N. J.; Waite, J. H.; Butler, A.; Israelachvili, J. N., Defining the Catechol–Cation Synergy for Enhanced Wet Adhesion to Mineral Surfaces. J. Am. Chem. Soc. 2016, 138, (29), 9013-9016.
69. Assunção-Miranda, I.; Cruz-Oliveira, C.; Neris, R. L. S.; Figueiredo, C. M.; Pereira, L. P. S.; Rodrigues, D.; Araujo, D. F. F.; Da Poian, A. T.; Bozza, M. T., Inactivation of Dengue and Yellow Fever viruses by heme, cobalt-protoporphyrin IX and tin-protoporphyrin IX. J. Appl. Microbiol 2016, 120, (3), 790-804.
70. Singh, J.; Srivastav, A. N.; Singh, N.; Singh, A., Stability Constants of Metal Complexes in Solution. In Stability of Coordination Compounds, IntechOpen: 2019.
71. Anotai, J.; Lu, M.-C.; Chewpreecha, P., Kinetics of aniline degradation by Fenton and electro-Fenton processes. Water Res. 2006, 40, (9), 1841-1847.

Table of Contents